Electronic Supplementary Information to

Atomic Structure and Water Arrangement on K-Feldspar Microcline (001)

Tobias Dickbreder,[†a] Franziska Sabath,[†a] Bernhard Reischl,[b] Rasmus V. E. Nilsson,[b] Adam S. Foster,[c,d] Ralf Bechstein[a] and Angelika Kühnle[a]

[a] Faculty of Chemistry, Physical Chemistry I, Bielefeld University, 33615 Bielefeld, Germany.

[b] Institute for Atmospheric and Earth System Research (INAR)/Physics, Faculty of Science, University of Helsinki, 00014 Helsinki, Finland.

[c] Department of Applied Physics, Aalto University, Finland.

[d] Nano Life Science Institute (WPI-NanoLSI), Kanazawa University; Kanazawa 920-1192, Japan.

[†] These authors contributed equally.

X-ray diffraction data

Table S1 shows the X-ray diffraction data obtained from the crystals used in this study together with the unit cell dimensions from our DFT and MD calculations. Two different crystals were used in this work. One crystal is referred to as MI-UHV-4b, which exhibits a white opaque color and which was used for the UHV experiments. A second crystal, labelled Mi-I, was used for the investigation carried out at the mineral-water interface. The latter crystal is transparent and colorless. We also provide the dimensions from literature for fully ordered microcline (maximum microcline) as a reference [1].

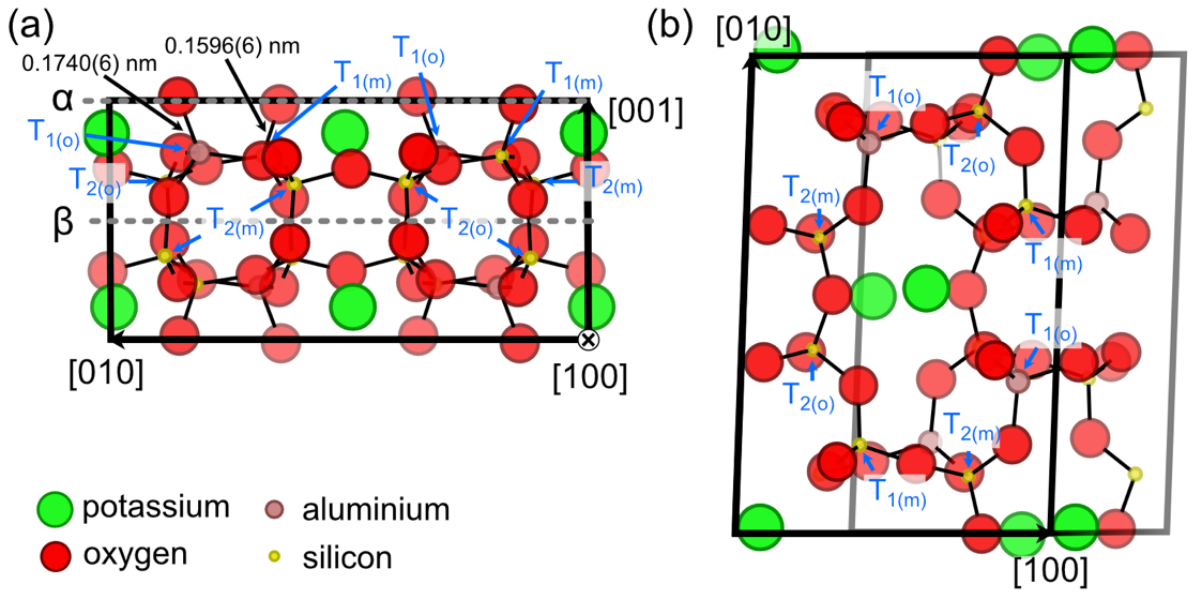

Figure S1. Bulk structure of K-feldspar microcline sample Mi-UHV-4b as determined by XRD. (a) shows a side view on the (001) crystal plane along the [100] direction. (b) is a top view on the (001) crystal plane. In both views, all atoms contained within the unit cell of monoclinic feldspar are displayed. The depth of atoms is encoded with an opacity axis. Positions of the four distinct tetrahedral sites $T_{1(o)}$, $T_{1(m)}$, $T_{2(o)}$ and $T_{2(m)}$ are indicated by labels. The lengths of the Al-O and Si-O bonds determined by XRD are also given.

Table S1. Comparison of XRD unit cell dimensions obtained from the crystals used in this work, DFT and MD parameters from this study and literature values for maximum microcline [1].

	MI-UHV-4b	**Mi-I**	**DFT**	**MD**	**Finney1964**
K	0.93	0.93			
Na	0.07	0.07			
a / Å	8.5606	8.5628	8.581	8.578	8.5726
b / Å	12.9848	12.9510	13.064	12.960	12.9618
c / Å	7.2227	7.2098	7.270	7.211	7.2188
α / °	90.584	90.223	90.61	90.30	90.34
β / °	115.968	115.981	115.70	116.03	115.55
γ / °	87.955	89.030	87.62	89.12	87.45
Al occ. $T_{2(o)}$	0.060	0.013	0	0	0.06
Al occ. $T_{1(m)}$	0.106	0.119	0	0	0.02
Al occ. $T_{2(m)}$	0.086	0.099	0	0	0.00
Al occ. $T_{1(o)}$	0.848	0.762	1	1	0.90

Further DFT data

Figure S2 shows the full slab used for the DFT calculations of the as-cleaved and hydroxyl-terminated microcline (001) surface.

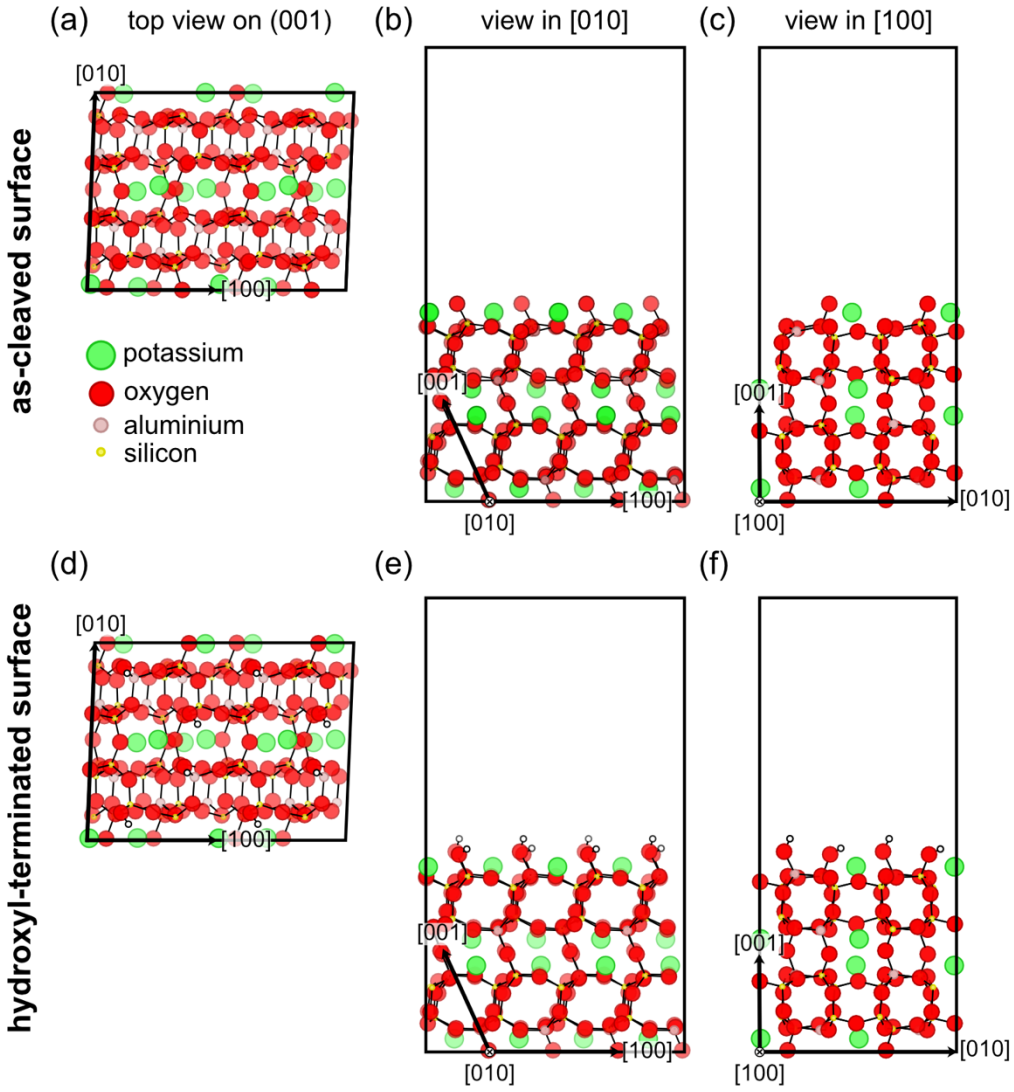

Figure S2. Full DFT structures of the as-cleaved (a-c) and hydroxyl-terminated (d-f) microcline (001) surface. Shown are the top views on the (001) plane (a+d) as well as side views along the [010] (b+e) and [100] (c+f) directions. The depth of the displayed atoms orthogonal to the viewing plane is encoded with an opacity axis. The $\mathbf{2 \times 1 \times 2}$ supercell is indicated by black boxes.

Further AFM data taken in UHV

Figure S3 reveals more information about the AFM image shown in Figure 2. In the AFM image in Figure S3 (a), the contrast varies slightly in the image with an especially pronounced contrast in a band from the top left to the bottom right corner. Part of the areas with the especially pronounced and more muted contrast are marked by a red and blue square, respectively. The comparison of the Fourier transform of the complete image (Figure S3 (c)) with the Fourier transforms of the red and blue areas (Figure S3 (d) and (e)) shows that the periodicity is identical throughout the whole image. Moreover, the z-piezo displacement channel of the image shown in Figure 32 (a) is shown in (b). Figure S3 (b) shows that the area with a slightly muted contrast appears to be around 0.2 nm higher than the rest of the image. This height difference is too small for a monoatomic step edge, which would exhibit a height of 0.65 nm. We currently do not know where this height difference originates from.

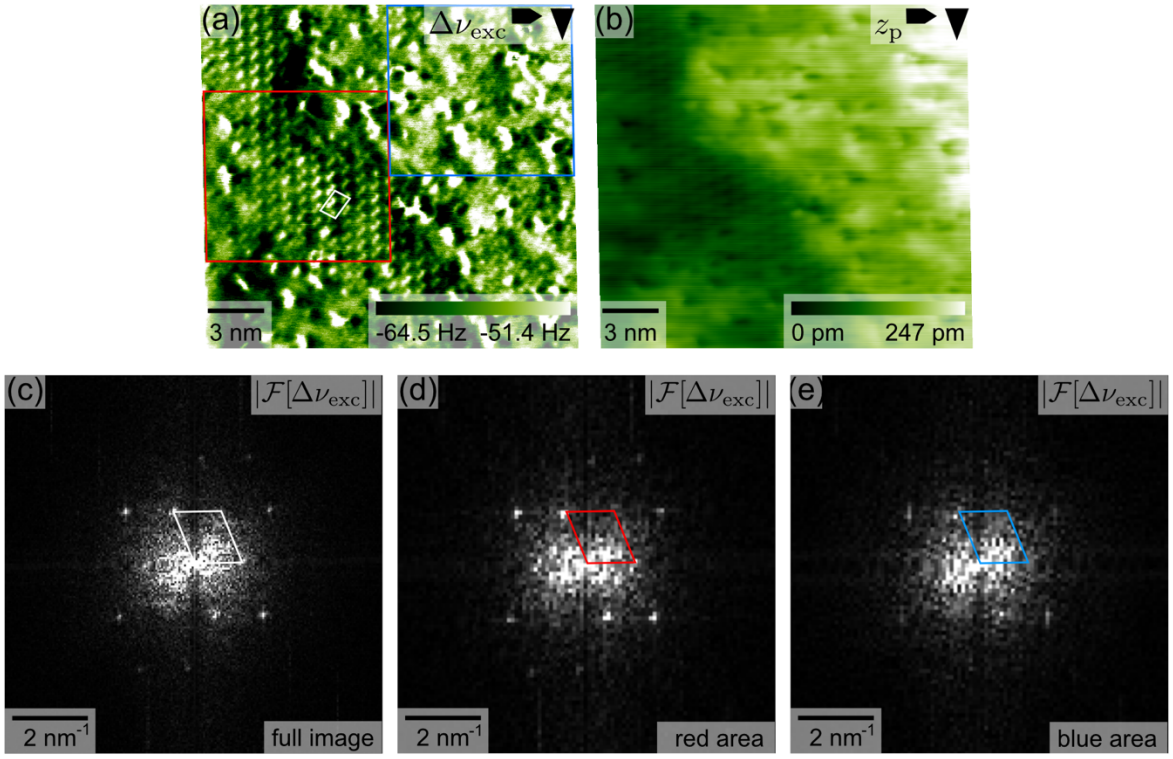

Figure S3. High-resolution AFM images taken on microcline (001) under UHV conditions. (a) and (b) show the excitation frequency shift and *z*-piezo displacement of the same atomic resolution image shown in fig. 2 (c) and (d). The two-dimensional Fourier transform of the full AFM image in (b) is shown in (c), and the Fourier transforms of the red and blue areas in (a) are shown in (d) and (e), respectively. In all Fourier transforms the primitive unit cell derived from the Fourier transform of the full image is marked with a quadrangle. All images and Fourier transforms are calibrated and corrected for linear drift.

Figure S4 shows further AFM data taken in UHV that exhibit a different contrast than the pronounced contrast shown in the main text. The unit cell dimensions, however, agree with those discussed in the main text within the experimental error. We think that the difference in atomic contrast is induced by a different termination of the AFM tip.

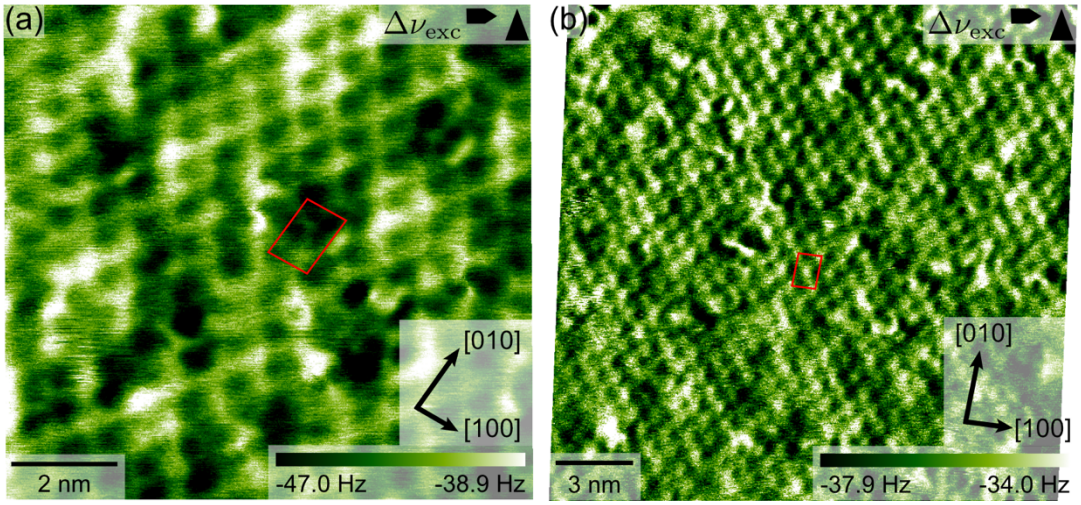

Figure S4. High-resolution AFM images taken on microcline (001) under UHV conditions showing the second and third atomic-resolution contrasts. All images are calibrated and corrected for linear drift. The unit cells and directions were derived from the 2D Fourier transforms.

Further 3D AFM slices

Figure S5 shows further slices through a 3D AFM map. The lateral slices (see Fig. S5 (a) – (c)) were extracted parallel to the (001) microcline surface at the positions of the peaks (1), (2) and (3) (see Fig. 4 (c)). In addition, Fig. S5 (d) shows the autocorrelation of the lateral slice at position (3). In the lateral slice at position (1), *i. e.*, very close to the (001) microcline surface, no contrast can be obtained. Unlike the lateral slice close to the surface, the lateral slices further away at positions (2) and (3) (see Fig. S5 (b) and (c)) show a periodic structure that are closely similar to the periodic structure obtained by two-dimensional AFM in Fig. 4 (a). Due to a lower amount of points and lines in 3D AFM maps (64 x 114 px^2) in contrast to 2D AFM images (512 x 512 px^2) the structure is less distinguishable in the lateral slices in Fig. S5 (b) and (c) compared to Fig, 4 (a). Two representative $\Delta\nu_{exc}$ vs. z_p+q_s profile positions A (red) and B (blue) are highlighted with circles in Fig. S5 (b) and (c). The autocorrelation image in Fig. S5 (d) of the lateral slice at position (3)

shows the periodic structure of the lateral slice more easily. Therein, the unit cell is marked by the red quadrangle and contains as well as in 2D AFM images two bright features.

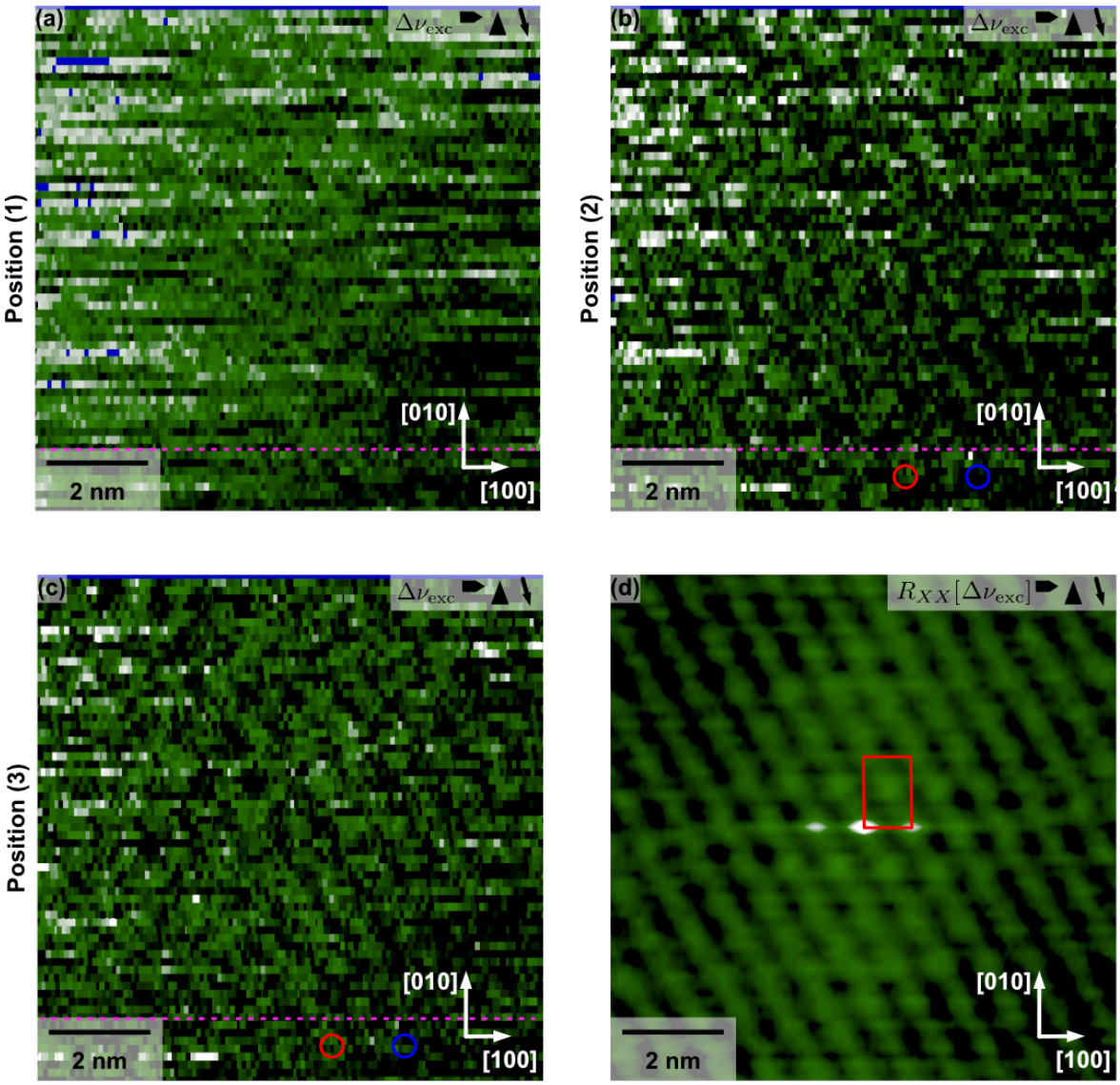

Figure S5. (a) – (c) Lateral slices through a 3D AFM data set taken at the (001) microcline-water interface on the corresponding z_p+q_s positions in fig. 4 (c). Representative positions A (red) and B (blue) are highlighted in (b) and (c). The dashed magenta line in (a) – (c) displays where the slice normal to the surface shown in Fig. 4 (b) was extracted. The unit cell shown in (d) is derived by the autocorrelation image of position (3).

Further MD data

Figure S6 shows the time evolution of the occupancy of surface K^+ ion sites in a 140 ns MD simulation of the microcline (001)-water interface, starting from a bulk-terminated surface at time t = 0. As this is the slowest interfacial process, we determine that after t = 35 ns, the system has reached equilibrium, and interfacial properties can be determined from time averaging over the remaining 105 ns of the MD trajectory. Figure S7 shows the radial distribution functions (RDF), g(r), of water oxygen atoms around surface K^+ ions and hydroxyl oxygen atoms in the simulation. The average coordination number, n_c, is obtained by integrating the RDF from r = 0 to the minimum after the first peak, r_m: $n_c = \int_0^{r_m} 4\pi r^2 g(r)\, dr$. With values of r_m = 0.35 nm, and 0.31 nm, identified for K^+ ions and hydroxyl oxygens, respectively, we obtain coordination numbers of about 1.8, 2.0, and 2.5, for K^+ ions, silicon hydroxyls, and aluminium hydroxyls, respectively. Figure S8 shows the "survival probabilities", $P_i(t)$, of water molecules coordinating surface K^+ ions or hydroxyl groups. Following the method of De La Pierre et al. [2], the survival probabilities were calculated as $P(t) = \int_0^{\infty} E(t')\, dt'$, where E(t) dt represents the probability of a water molecule to remain coordinated to a surface site for a time between t and t + dt. P(t) is then fitted with the sum of two exponentially decaying functions, $P(t) = \sum_{j=1}^{2} a_j \exp(-t/\tau_j)$. The first time scale, τ_1, is very short and corresponds to fluctuations in and out of the cut-off radius, while the time scale for actual water exchange corresponds to τ_2. Figure S9 shows density isosurface maps of the different atomic species at the unconstrained microcline (001)-water interface. Figure S10 shows the differences at the microcline (001)-water interface, when surface K^+ ions are free to go into solution, or constrained to remain at the mineral surface.

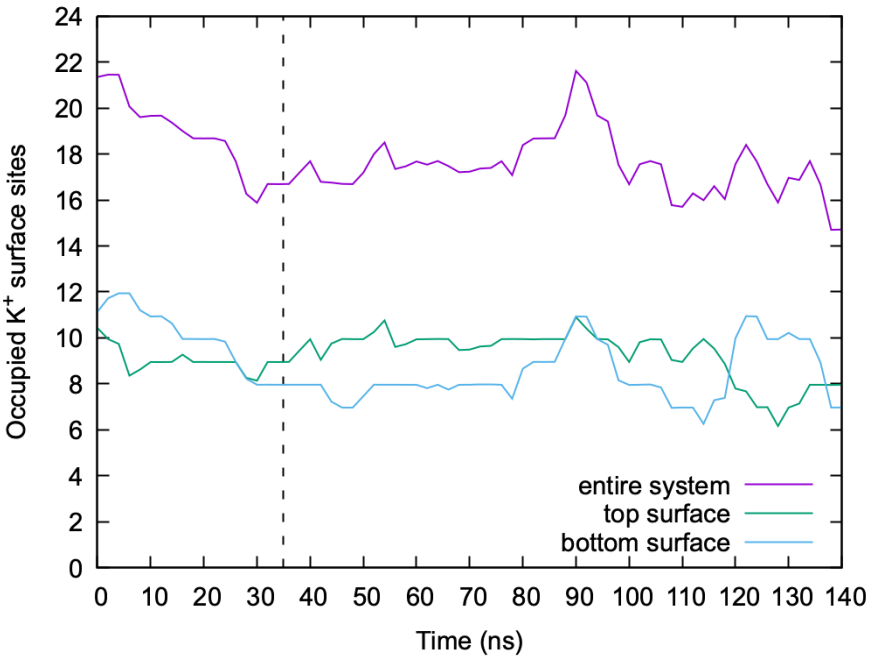

Figure S6. Time evolution of the surface K^+ site occupancy in the simulation over the 140 ns trajectory, block averaged over 2 ns (full lines). The dashed black line indicates the end of the 35 ns equilibration period and marks the start of the 105 ns used for analyses of interfacial properties.

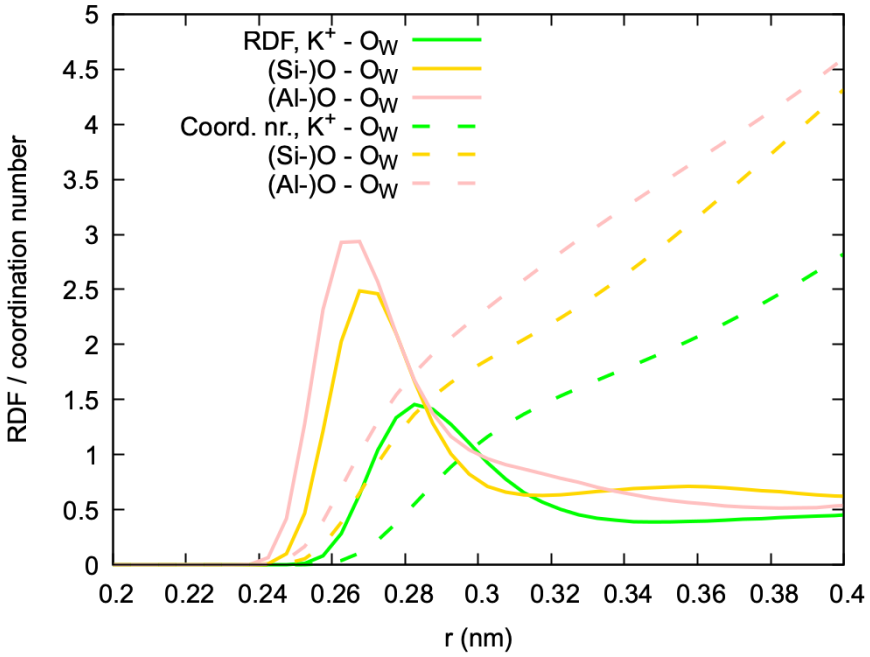

Figure S7. Radial distribution functions (RDF) for K^+ ions, or hydroxyl oxygen atoms, and water oxygen atoms, O_W (full lines). Integrating the RDF over the radial distance r yields the coordination numbers (dashed lines). Note that the RDFs do not converge to 1 with increasing r, as the reference sites are located on the mineral surface, not in bulk solution.

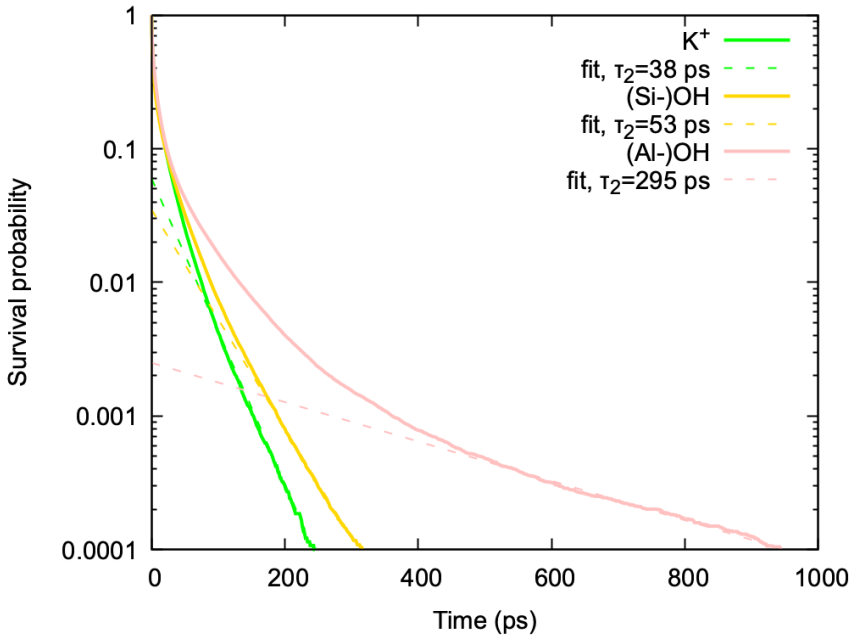

Figure S8. Survival probabilities $P_i(t)$ of water molecules in the first coordination shell of surface K^+ ions, and hydroxyl groups on surface Si or Al atoms (full lines). The timescales for water exchange are obtained from linear fits to the logarithm of $P_i(t)$ (dashed lines)

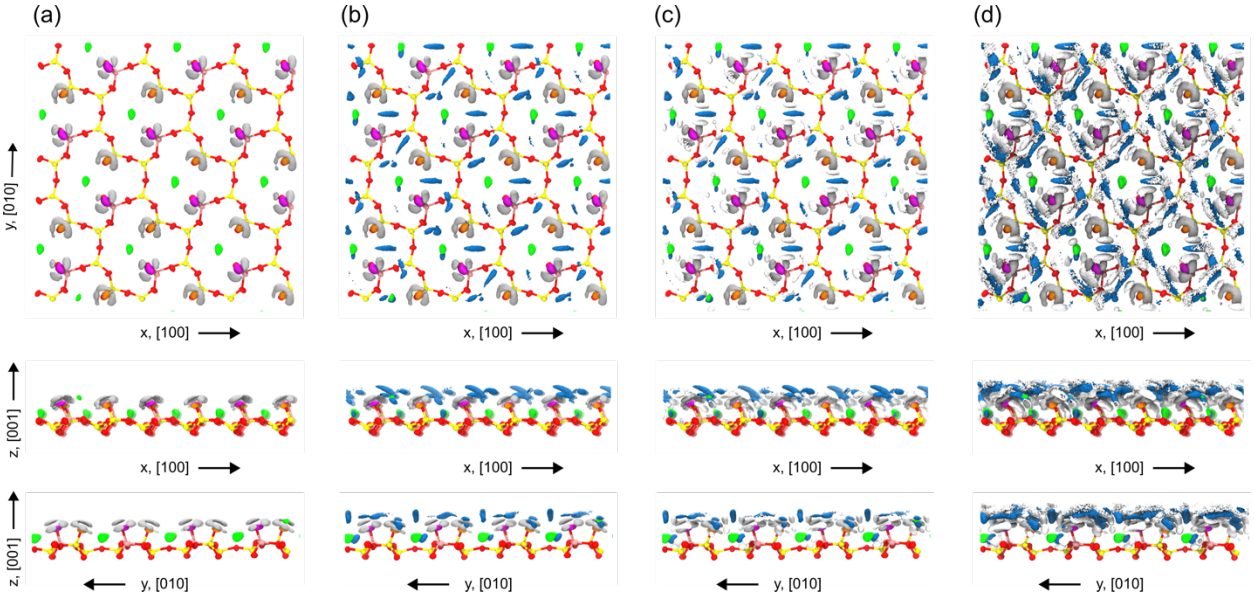

Figure S9. Density isosurface maps at $\rho = 100\rho_0$ ($\approx$ 3370 nm^{-3}) of the different atomic species at the microcline (001)-water interface, averaged over a 105 ns MD trajectory. Column (a) shows the hydroxylated mineral surface only, (b) includes water oxygens, and (c) includes water oxygens and hydrogens. Column (d) shows water oxygen and hydrogen density isomaps at $\rho = 50\rho_0$ ($\approx$1685 nm^{-3}) for comparison. K^+ is green, Si yellow, Al pink, bridging O red, hydroxyl O on Si orange, hydroxyl O on Al magenta, hydroxyl H grey, water O blue, and water H white. Bonds between Si, O, and Al atoms in the microcline (001) surface layer are indicated by lines.

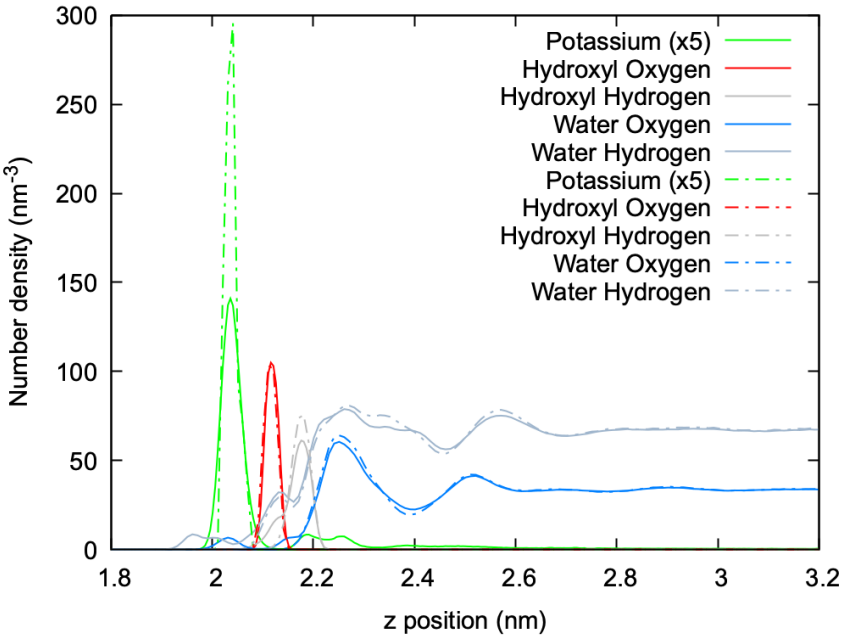

Figure S10. Number densities of different atomic species at the microcline (001)-water interface. Full lines are obtained in simulations with free K^+ ions (identical to the data in Fig. 3 (b) in the main paper), whereas the dot-dashed lines are obtained in simulations where K^+ ions are restrained to their surface positions with a harmonic potential. Potassium densities have been multiplied by 5 for better visualization.

References

[1] J.J. Finney, S.W. Bailey, *Z. Kristallogr. – Cryst. Mater.* **119** (1964) 413.
[2] M. De La Pierre, P. Raiteri and J. D. Gale, *Cryst. Growth Des.,* 2016, **16**, 5907−5914.